Dynamics of Glyphosate-Induced Conformational Changes of *Mycobacterium tuberculosis* 5-Enolpyruvylshikimate-3-phosphate Synthase (EC 2.5.1.19) Determined by Hydrogen−Deuterium Exchange and Electrospray Mass Spectrometry†

Maurício R. Marques,‡ Alessandra Vaso,‡ João Ruggiero Neto,§ Marcelo A. Fossey,§ Jaim S. Oliveira,|| Luiz A. Basso,|| Diógenes S. dos Santos,*,⊥ Walter F. de Azevedo Junior,# and Mario S. Palma*,‡

Laboratory of Structural Biology and Zoochemistry, CEIS/Department of Biology, Institute of Biosciences, UNESP, Rio Claro, SP 13506-900, Brazil, Departamento de Física, IBILCE−Unesp, São José do Rio Preto, SP 15054-000, Brazil, Rede Brasileira de Pesquisas em Tuberculose Grupo de Microbiologia Molecular e Funcional, Departamento de Biologia Molecular e Biotecnologia, UFRGS, Porto Alegre, RS 91501-970, Brazil, Centro de Pesquisas em Biologia Molecular e Funcional/PUCRS, Avenida Ipiranga 6681, Tecnopuc, Partenon 90619-900, Porto Alegre, RS, Brazil, and Faculdade de Biociências−PUCRS, Av. Ipiranga, 6681, Porto Alegre, RS CEP90619-900, Brazil

Received January 23, 2008; Revised Manuscript Received May 19, 2008

ABSTRACT: The enzyme 5-enolpyruvylshikimate-3-phosphate synthase (EPSPS) catalyzes the reaction between shikimate 3-phosphate and phosphoenolpyruvate to form 5-enolpyruvylshikimate 3-phosphate, an intermediate in the shikimate pathway, which leads to the biosynthesis of aromatic amino acids. EPSPS exists in an open conformation in the absence of substrates and/or inhibitors and in a closed conformation when bound to the substrate and/or inhibitor. In the present report, the H/D exchange properties of EPSPS from *Mycobacterium tuberculosis* (*Mt*) were investigated for both enzyme conformations using ESI mass spectrometry and circular dichroism (CD). When the conformational changes identified by H/D exchanges were mapped on the 3-D structure, it was observed that the apoenzyme underwent extensive conformational changes due to glyphosate complexation, characterized by an increase in the content of α-helices from 40% to 57%, while the *β*-sheet content decreased from 30% to 23%. These results indicate that the enzyme underwent a series of rearrangements of its secondary structure that were accompanied by a large decrease in solvent access to many different regions of the protein. This was attributed to the compaction of 71% of α-helices and 57% of *β*-sheets as a consequence of glyphosate binding to the enzyme. Apparently, *Mt*EPSPS undergoes a series of inhibitor-induced conformational changes, which seem to have caused synergistic effects in preventing solvent access to the core of molecule, especially in the cleft region. This may be part of the mechanism of inhibition of the enzyme, which is required to prevent the hydration of the substrate binding site and also to induce the cleft closure to avoid entrance of the substrates.

One of the great challenges of modern medical research is the development of new drugs to face infectious diseases caused by pathogenic bacteria and protozoans, especially in developing and poor countries.

Tuberculosis remains as one of the most deadly infectious diseases in the world. It is estimated that about 1 billion individuals are infected with latent tuberculosis, which currently kills more than 2 million people every year worldwide (*1*). *Mycobacterium tuberculosis* is by far the biggest killer among infectious agents, accounting for 7% of all deaths and 26% of avoidable deaths (*1, 2*). The treatment of active cases of tuberculosis is a serious problem of chemotherapy, since it requires the simultaneous use of two or more frontline drugs, such as isoniazid, ethambutol, rifampicin, and streptomycin (*1*). Recent outbreaks of tuberculosis caused by multidrug-resistant (MDR) strains, mainly in individuals infected with HIV, have raised concerns and called global attention to the expanding current programs to develop new drugs that are based on the principle of selective inhibition of enzymes from resistant *M. tuberculosis* strains (*2*).

However, the reduced number of target macromolecules limits progress toward the development of novel drugs. Therefore, the identification of candidates for new antibiotic targets is of immense importance for the development of new antibiotics to combat multiresistant Gram-positive pathogens (*3, 4*). The shikimate pathway synthesizes aromatic amino acids, *p*-aminobenzoic acid, and other essential metabolites, such

† This work was supported by grants from FAPESP and Millennium Institute, MCT/CNPq. M.S.P., D.S.S., W.F.A.J., J.R.N., and L.A.B. are research awardees from the National Council for Scientific and Technological Development (CNPq).

* Corresponding authors. M.S.P.: phone/fax, +55 (19) 3526 4163; e-mail, mspalma@rc.unesp.br. D.S.S.: e-mail, diogenes@pucrs.br.

‡ Laboratory of Structural Biology and Zoochemistry, CEIS/Department of Biology, Institute of Biosciences, UNESP.

§ Departamento de Física, IBILCE−Unesp.

|| Rede Brasileira de Pesquisas em Tuberculose Grupo de Microbiologia Molecular e Funcional, Departamento de Biologia Molecular e Biotecnologia, UFRGS.

⊥ Centro de Pesquisas em Biologia Molecular e Funcional/PUCRS.

Faculdade de Biociências−PUCRS.

10.1021/bi800134y CCC: $40.75
Published on Web 06/18/2008

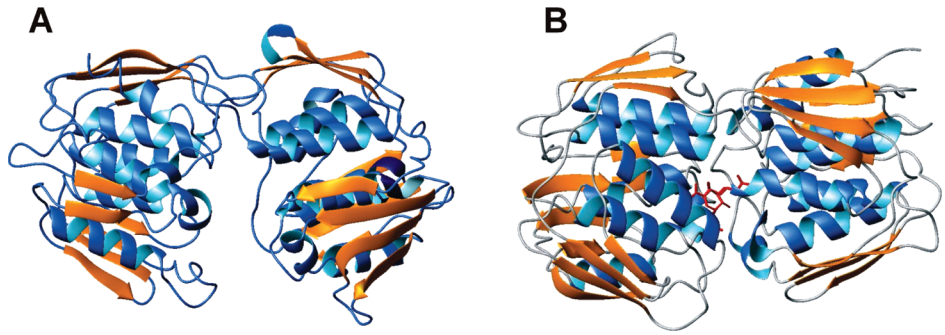

FIGURE 1: Ribbon diagram of the three-dimensional structures of the apo-*Mt*EPSP (PDB ID 2bjb) (A) and of the glyphosate-bound *Mt*EPSPS (B) generated by Molscript as described elsewhere (*2*).

as ubiquinone, menaquinone, and vitamin K. In a sequence of seven metabolic steps, phosphoenolpyruvate and erythrose 4-phosphate are converted to chorismate, the precursor of the aromatic amino acids and many aromatic secondary metabolites. All of the pathway intermediates can also be considered branch point compounds that may serve as substrates for other metabolic pathways. The shikimate pathway, which has been found in plants, algae, bacteria, and fungi, was also recently detected in several apicomplexan parasites (*5, 6*); however, this pathway has not been found in mammals to date. The indispensability of this pathway for bacterial and protozoan survival and the large amounts of literature data about the cloning and purification of the seven enzymes from prokaryotic and eukaryotic sources make these enzymes very attractive targets for the development of inhibitors that have large potential to become powerful and selective biocide drugs against human pathogens.

In the sixth step of the shikimate pathway, the enzyme 5-enolpyruvylshikimate-3-phosphate synthase (EPSPS) (EC 2.5.1.19) catalyzes the reaction between shikimate 3-phosphate (S3P) and phosphoenolpyruvate (PEP) to form 5-enolpyruvylshikimate 3-phosphate (EPSP), an intermediate of the shikimate pathway, which leads to the biosynthesis of aromatic amino acids (*7*). EPSPS is a monomeric enzyme with a molecular mass around 46 kDa. The enzyme has been purified from prokaryotes and eukaryotes, and the 3-D structure of *Escherichia coli* (*Ec*) EPSPS has been determined through X-ray crystallography, which indicated that it has two domains with the active site near the interdomain crossover segment (*7*).

The structure of unliganded *Mt*EPSPS was determined by crystallography (*8*), while the form bound to its inhibitor was modeled using structural bioinformatics (*2*). EPSPS occurs in an open conformation in the absence of substrates/inhibitor and in a closed conformation when bound to the substrates/inhibitor (*7*) (Figure 1). Each domain is composed of three copies of $\beta\alpha\beta\alpha\beta\beta$-folding units; the four-stranded β-sheet structures of each unit contain both parallel and antiparallel strands, while the helices are parallel. The two-domain structure of the apoenzyme has a distinctive fold that is formed by 6-fold replication of protein folding units, each one formed by two parallel α-helices and the four-stranded β-sheets (Figure 2 A). The structural units are related by an approximate 3-fold symmetry axis; in each domain, three of the helices are completely buried by a surface formed by the three sheets and solvent-accessible faces of the other helices (*9*).

The topological 3-fold symmetry and orientation of each of the two observed globular domains may direct the binding

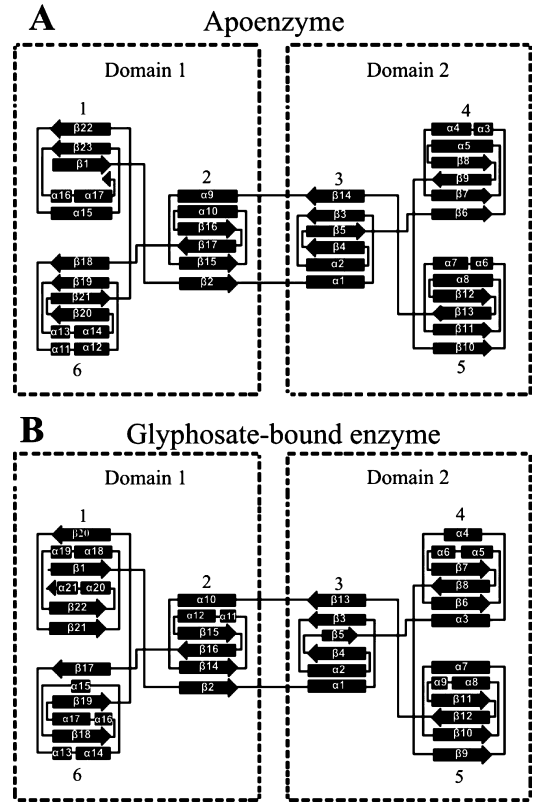

FIGURE 2: Schematic illustration of the backbone of *Mt*EPSPS and the order of the principal secondary structural elements, as they occur in the enzyme molecule, both for the apoenzyme (A) and the glyphosate-bound enzyme (B). The open form of the enzyme contains two domains (1 and 2); each domain is composed of three copies of $\beta\alpha\beta\alpha\beta\beta$-folding units in the apoenzyme (A). The four-stranded β-sheet structures of each unit contain both parallel and antiparallel strands, while the helices are parallel. The two-domain structure of the apoenzyme has a distinctive fold that is formed by 6-fold replication of protein folding units, each one formed by two parallel α-helices and a four-stranded sheet (A). Domain 1 is constituted of units 1, 2, and 6 of $\beta\alpha\beta\alpha\beta\beta$-folds, and domain 2 is constituted of three other $\beta\alpha\beta\alpha\beta\beta$-folding units, designated 3, 4, and 5. The representation for the inhibitor-bound enzyme (B) reveals some structural rearrangements. The structural pattern was slightly modified after inhibitor binding to the enzyme; units 1, 2, 3, and 5 maintained the $\beta\alpha\beta\alpha\beta\beta$-fold, while units 4 and 6 presented a $\beta\alpha\beta\alpha\beta\alpha$-fold. Some elements of α-helices split into two parts, while others merged into a single one, as a result of conformational changes induced by glyphosate binding to the enzyme.

of substrates and inhibitors by a helix macrodipole effect, implying that the active site is located near the interdomain crossover segments (*7*). The domains are approximately hemispheric, each with a radius of about 21 Å. The domains are linked by two crossover chain segments with both the

amino and carboxyl termini of the protein in the lower domain. The two flat surfaces of the hemispheres, which project to form a "V", are almost normal and accommodate the amino termini of the six helices in each domain with their N-termini oriented toward the cleft between the domains, suggesting the possibility that the resulting macrodipole may direct the negatively charged substrates into the cleft where the reaction occurs (*2, 10*).

The catalytic mechanism of this enzyme has been the subject of many investigations, while the enzyme−substrate complexes and intermediate states have been characterized by different spectroscopic techniques (*11–17*). This enzyme is inhibited by the compound *N*-(phosphonomethyl)glycine, also known as glyphosate, the broad-spectrum active principle of the nonselective herbicides RoundUp and Touch-Down, which inhibits bacterial growth *in vitro* (*18*); this compound constitutes a molecular model system for the rational development of other EPSPS inhibitors (*17*).

This enzyme also constitutes an attractive target for the development of antimicrobial and antiparasitic drugs, since the shikimate pathway is absent from mammals but is essential for the survival of microorganisms. A variety of derivatives of glyphosate are currently being used to elucidate the structure−function relationship for inhibitors of EPSPS (*19*); hundreds of analogues of glyphosate have been synthesized and tested for inhibition of the enzyme; however, none of them were more potent than glyphosate (*20*). Efforts made to understand the mode of action of this inhibitor have inspired the search for other compounds with similar inhibitory capabilities (*21*). Such a type of compound may be considered safe for humans, and they could potentially be used as a therapeutic agent against pathogenic bacteria and/or protozoans in reasonable concentrations (*1*).

Park et al. (*4*) proposed that the EPSPS domains, in the unbound state, present a "dynamic motion" that is in equilibrium between the open and closed conformations (Figure 1). S3P binds to *Ec*EPSPS, but it is unable to induce the domains closure by itself, since the variation of entropy of this interaction is positive (*22*). In contrast, glyphosate binding to the *Ec*EPSPS−S3P complex induces a high negative entropy variation, suggesting an extensive conformational change accompanied by protein reorganization with loss of flexibility. These data suggest that the binding of glyphosate may induce the closing of *Ec*EPSPS. The analysis of the entropy variation suggests that inorganic phosphate (P_i) is able to induce the closure of the preformed *Ec*EPSPS−S3P complex similar to glyphosate (*22*). This information reinforces that the compact state of the enzyme described above may be due to P_i binding; it must be emphasized that P_i may possess multiple binding sites in the EPSPS cleft, probably due to the many positive charges on their domain interface (*23*). Knowledge regarding the dynamics of the structural changes of the enzyme as a result of its interaction with different ligands will certainly contribute to a better understanding of the physicochemical properties of these interactions and provide new insights for the rational development of novel antimicrobial agents.

The hydrogen/deuterium (H/D) exchange properties of peptide amide hydrogens can reflect protein dynamic features, and the monitoring of H/D exchange has been used to probe protein−ligand interactions (*24*). Presumably, solvent can access flexible or dynamic regions of a protein more readily, and such events are reflected by fast deuterium exchange. Regions of limited flexibility may be less penetrable by solvent; however, slow deuterium exchange may also be a reflection of greater stability of the hydrogen bonds. Regardless, structural changes occurring in a protein as a consequence of ligand binding should be evident in analysis of the H/D exchange behavior. Detecting amide deuterium exchange information by mass spectrometry is a powerful technique that provides an experimental approach for examining solvent accessibility of the protein backbone amide hydrogens and may therefore provide information about the environment of distinct regions of the protein and how that environment is affected by the binding of ligands (*25–28*).

Considering that the interactions of EPSPS−glyphosate are strongly influenced by induced fit and that even minor conformational changes may result in a dramatic reduction of the potency of enzyme inhibition (*29*), the present paper reports the H/D exchange properties of *Mt*EPSPS both for the apoenzyme and for the glyphosate-bound enzyme, in order to investigate the inhibitor-induced conformational changes. When the conformational changes identified by H/D exchange are mapped on the 3-D structure and/or along the secondary structures of both conformations of *Mt*EPSPS, these results may contribute to a more complete understanding of the enzyme−inhibitor interaction.

MATERIALS AND METHODS

Protein Sample. The active recombinant *Mt*EPSPS was expressed and purified as described elsewhere (*30, 31*). The protein pellet from a saturated 80% (w/v) ammonium sulfate solution was resolubilized and dialyzed exhaustively against 5 mM sodium phosphate, pH 6.9. The protein concentration was determined spectrophotometrically using the calculated extinction coefficient for native conditions or for denatured proteins (*32*). Glyphosate [*N*-(phosphonomethyl)glycine] was acquired from Monsanto.

H/D Exchange, Peptic Digestion, and Mass Spectrometry. The intact protein samples were injected through a reversed-phase column, POROS 10R2 (100 × 0.25 mm; Perceptive Biosystems), under a flow rate of 50 μL/min; intact protein samples were eluted using a gradient of acetonitrile from 2% to 98% (v/v) (containing 0.05% (v/v) TFA) over the course of 8 min directly into the mass spectrometer ionization system.

The concentration of the *Mt*EPSPS stock solution was 1.5 mM in phosphate buffer (100 mM, pH 6.9, 25 °C). The enzyme in a final concentration of 75 μM was labeled by diluting the solution 20-fold with D_2O (5 mM sodium phosphate, pD 6.9, 25 °C); when necessary, the incubation in the presence of the inhibitor, glyphosate, in a final concentration of 2600 μM was solubilized in the medium described above. Solutions were maintained at room temperature (25 °C), and the time of isotope exchange ranged from 1 min to 8 h. All pH and pD values reported were taken directly with a pH meter and were not corrected for isotope effects. At each time point, aliquots (20 μL, 30 nmol) were taken out of the exchange tube and quenched by mixing the solution with a 1:1 ratio of the quenching buffer (D_2O, 100 mM sodium phosphate, pD 2.5) and cooled to 0 °C in order to slow down the H/D exchange. Immediately after quenching had been carried out, exchanged *Mt*EPSPS

aliquots were digested for 5 min at 0 °C by adding 1 μL of a precooled pepsin solution (1 mg/mL in 5% (v/v) formic acid). Aliquots (5 μL) were taken from the digest and loaded onto a microbore HPLC column (20 cm × 0.32 mm, 15 μm, LUNA C18) in an ice bath. The peptic peptides were separated over a 10 min period with a 2−65% acetonitrile/water gradient (containing 0.05% (v/v) TFA). The column effluent (30 μL/min) was delivered directly to the mass spectrometer for ESI-MS and ESI-MS/MS experiments.

Using PEEK tubing (1/16 in. o.d. × 0.25 mm i.d. Blue (0.010 in.); Micromass), the HPLC system was connected directly to the ESI probe of the mass spectrometer. A flow of 80 μL/min to the ESI probe was obtained by splitting a primary flow of 600 μL/min by means of a T-piece, allowing the compounds to be monitored and their molecular masses to be determined. The LC eluents were analyzed by positive electrospray ionization (ESI^+). The MS experiments were performed by using an ESI triple quadrupole instrument, model Quatro II (Micromass, UK), in the continuous acquisition mode; a capillary voltage of 3.5 kV, a cone voltage of 30 V, and a desolvation gas temperature of 80 °C were used. The masses were calibrated with intact horse heart myoglobin, and its typical cone voltage induced fragments. The ESI spectra were obtained in the continuous acquisition mode, scanning from *m*/*z* 100−2500 with a scan time of 6 s. The spectral data were acquired and monitored using the MassLynx software (Micromass).

Peptides were sequenced online using ESI^+-MS/MS under the LC conditions described above. Typical conditions were a capillary voltage of 3 kV, a cone voltage of 30 V, a collision gas pressure of 3.5×10^{-3} mbar, and a desolvation gas temperature of 80 °C. The singly charged protonated molecules of the precursors were selected in Q1 and subjected to collision-induced dissociation (CID) with argon gas at a 50 eV collision energy; the product ions were detected by scanning Q3. All of the MS/MS experiments were performed using an ESI triple quadrupole instrument, model Quatro II (Micromass, U.K.), in continuous acquisition mode, scanning from *m*/*z* 40 to the *m*/*z* value of the $[M + H]^+$ ion of each peptide, with a scan time of 5 s. The spectral data were acquired and monitored using the MassLynx software. Peptide sequences were assigned manually from the ESI^+-MS/MS product ion mass spectra with the help of the MaxEnt1 software (Micromass, U.K.).

Mass spectrometry analyses of all samples within each comparison set were done on the same day, with the same instrumental conditions. Deconvolution of the intact protein spectra was performed with the program Transform (Waters). The error of each data point for the intact protein was determined to be 0.3 Da (based on multiple measurements).

Since protic solvents were used in the HPLC protocols, labile deuterons both in side chains and in the N- and C-terminal ends were replaced by protons. Deuterium back-exchange from amide linkages was minimized by cooling the chromatographic system to 0 °C, maintaining a pH of 2.5, and using a steep elution gradient. Two control samples were analyzed under the same conditions to assess the extent of exchange that occurred during analysis, despite maintaining the quench conditions. Results for these control samples, undeuterated protein ($m_{0\%}$), and totally exchanged protein ($m_{100\%}$) were used to adjust for the artificial exchange that occurred during analysis as described elsewhere (*33*). The undeuterated control sample was prepared by diluting a solution of *Mt*EPSPS into D_2O buffer under quench conditions (0 °C at pH 2.5).

The mass of each peptide was taken as the centroid mass of the isotopic envelope with the program MassLynx (Micromass, U.K.). In order to account for the exchange of deuterium during the HPLC step (back-exchange) and the use of only a 20-fold excess of D_2O during the labeling step, which limits the forward exchange reaction, an experimental correction is necessary. In our experiments, a 100% deuterated protein control was prepared by diluting the protein stock in the labeling solution and quenching buffer, incubating at 50 °C for 8 h, and then incubating at room temperature (approximately 25 °C) for 24 h.

Data were processed using the centroid isotopic distributions corresponding to the +1, +2, or +3 charge states of each deuterated peptide. The corrected extent of deuterium incorporation was calculated according to the equation (*33, 34*):

$$D = \frac{m - m_{0\%}}{m - m_{100\%}} N$$

where D is the number of amide hydrogen atoms incorporated in a specific peptide, m is the experimental centroid mass of the deuterated peptide at a certain time point, $m_{0\%}$ is the centroid mass of the undeuterated peptide, $m_{100\%}$ is the centroid mass of the 100% deuterated control peptide, and N is the number of amide hydrogens for each peptide characterized.

Thus, the deuterium level (D) at any peptic fragment amide linkage during the time course of incubation in the presence of D_2O is given by the equation (*35*):

$$D = N - N_{\text{fast}} e^{-k_{\text{fast}} t} - N_{\text{int}} e^{-k_{\text{int}} t} - N_{\text{slow}} e^{-k_{\text{slow}} t}$$

where N_{fast} is the number of fast exchanging amide hydrogen atoms, N_{int} is the number of intermediate exchanging amide hydrogen atoms, N_{slow} is the number of slowly exchanging amide hydrogen atoms, k_{fast}, k_{int}, and k_{slow} correspond to the respective exchange rate constants for the above-mentioned numbers of exchanging amide hydrogen atoms, and t is the specific time of enzyme incubation in presence of D_2O.

Kinetic plots of deuteration were typically fit to a double exponential model to account for deuterons exchanging at a rapid rate (mainly solvent-accessible amides) and those hindered by hydrogen bonding and/or solvent occlusion. Nonlinear least-squares fitting was implemented in Prism 4.0 (San Diego, CA).

Adjustments for a small amount of deuterium loss during digestion and HPLC protocols were made using results obtained for each of the control samples as described above. This artificial loss of deuterium was 15−20% in most peptides.

Circular Dichroism Spectroscopy. Circular dichroism (CD) measurements were performed in a Jasco J-810 spectropolarimeter with the temperature controlled by a Peltier-type control system PFD 425S. The *Mt*EPSPS protein was tested in sodium phosphate buffer at final concentrations of 200−2000 μg/mL. The spectra were collected using a 0.1 mm path length cell at a scanning rate of 100 nm/min with a spectral bandwidth of 1 nm. The resultant spectra were normalized to residual molar ellipticity ($[\nu]$), and the software CDNN Deconvolution (*36*) was used for estimating the

*Mt*EPSPS secondary structure content, in the presence and absence of enzyme inhibitor (glyphosate).

Molecular Models. A molecular model for *Mt*EPSPS was utilized to map the positions that underwent conformational changes under the experimental conditions described above. The open conformation model characteristic of the apoenzyme was generated using the atomic coordinates from 2BJB (http://www.rcsb.org/pdb/explore.do?structureId=2BJB), while the closed conformation model characteristic of the glyphosate-bound enzyme was the same one previously reported by Pereira et al. (*2*) and Borges et al. (*37*). Briefly, for modeling of the EPSP synthase we used restrained-based modeling implemented in the program PARMODEL (*38*). The degree of primary sequence identity between MtEPSP synthase and EPSP synthase from *E. coli* indicates that the crystallographic structures of EcEPSP are good models to be used as templates for MtESPS synthase. The atomic coordinates of all waters were removed from the EPSP structure.

The model of closed conformation was generated by using the α-carbon atomic coordinates from 1G6S (*39*). The atomic coordinates of all waters were removed from the EPSPS structure. The 3-phosphoshikimate and glyphosate of the template were kept in the structure for the closed conformation. Finally, the model was obtained by optimizing the objective function in Cartesian space. The optimization was carried out by the use of the variable target function method (*40*) employing methods of conjugate gradients. Several slightly different models can be calculated by varying the initial structure. A total of 1000 models were generated for each EPSPS conformation state, and the final models were selected based on stereochemical quality. All modeling processes were performed on a Beowulf cluster, with 16 nodes (B16/AMD Athlon 1800+; BioComp, São José do Rio Preto, SP, Brazil).

Calculation of SASA. The solvent-accessible surface area (SASA) was calculated using a grid-based method. A three-dimensional grid (1.0 Å spacing) covering the protein and its surroundings was created (*41–43*). Then, the accessibility of every grid point was calculated in the following way: all grid points lying within any of the protein atoms (defined from their van der Waals radii) were considered to be inaccessible to solvent; for all other grid points, a more thorough accessibility assignment was carried out. As an initial estimate, all of these grid points were considered to be solvent inaccessible. For each one of the grid points, the minimal distance to the van der Waals surface of the closest protein atom was calculated; if the value of the minimal distance was found to be longer than the probe radius (the probe radius of water was set to 1.4 Å), a sphere centered in the grid point with a radius of the minimal area was considered. All grid points lying within this sphere were set to water accessible. The SASA value of every atom was then calculated as the ratio between the accessible grid points in a shell around the atom to the total number of grid points in the shell. GETAREA (*44*), the algorithm used for this purpose, was validated with the web-based program from the Web site http://www.scsb.utmb.edu/getarea/areaman.html. The SASA values used in the present report refer only to the accessible surface of the backbone nitrogen.

Secondary structures and Hydrogen Bonding. The secondary structure of the protein was determined by the DSSP program; the virtual hydrogen-bonding sites were identified, and their number was determined using a method based on the positioning of the hydrogen atoms by optimizing hydrogen bond networks in protein structures (*45*). The calculations were performed with the algorithm WHAT IF, validated with the web-based program from the Web site http://swift.cmbi.ru.nl/servers/html/.

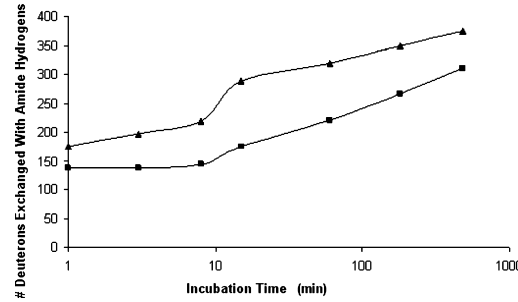

FIGURE 3: Time course of deuterium incorporation into *Mt*EPSPS both for the apoenzyme (▲) and for the glyphosate-bound enzyme (■) as a function of incubation at 25 °C and pH 6.9.

RESULTS

The crystallographic structure of *Mt*EPSPS has been recently solved (PDB access code 2BJB), and superposition of the homology model against the crystallographic structure shows rmsd below 0.5 Å after superposition, which validates the current homology model.

Structural changes enabling isotope exchange may involve global unfolding or minor fluctuations that allow exchange at individual amide linkages. The goal of this research was to determine the regions most accessible to the solvent, i.e., to identify and map the sequences most susceptible to conformational changes at the level of the 3-D structure of *Mt*EPSPS, including both the spontaneous structural changes occurring in the absence of the inhibitor and those induced by the binding of the inhibitor to the enzyme.

Taking into account the dissociation constant of the complex *Mt*EPSPS−glyphosate (K_d = 350 μM) under the experimental conditions described above, i.e., [apo-MtEPSPS] = 75 μM, [glyphosate] = 2600 μM, incubated at pH 6.9 and 25 °C, 87% of protein molecules are bound to the inhibitor before D_2O addition, while 26% of *Mt*EPSPS molecules were complexed with the inhibitor after 20-fold dilution with D_2O.

The Global H/D Exchange of MtEPSPS. The ESI-MS analysis of *Mt*EPSPS in its unliganded form revealed a molecular mass of 46427.6 Da (result not shown), which fits very well to the predicted value of 46427.7 Da. Low pH substantially reduces amide exchange rates, allowing the measurements prior to exchange events at physiological pH. Because deuterium labeling occurs when the protein is in its native state, the amount of deuteration reflects the solvent accessibility of certain protein regions. The rate and extent of the time-dependent deuterium incorporation was quantified by ESI^+-MS and plotted as a function of the incubation time course (Figure 3). The global deuterium incorporation increased slowly until 10 min at 25 °C, and after this time, both the apoenzyme and the glyphosate-bound enzyme presented a pronounced increase followed by a linear increase until 480 min of incubation. During this process, the apoenzyme was always more deuterated than the liganded

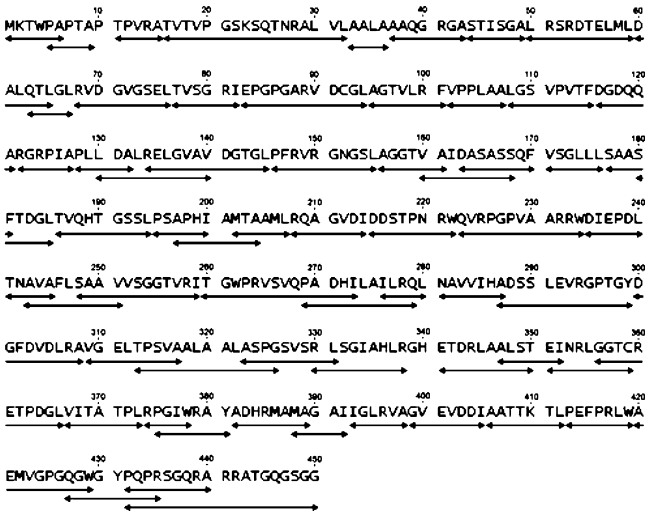

FIGURE 4: Map of peptic fragments used for H/D exchange analysis. The 67 fragments are indicated by double-headed arrows, covering 98.5% of the enzyme sequence.

enzyme. The number of deuterons exchanged after 1 min incubation at 25 °C was 173 for the apoenzyme and 135 for the inhibitor-bound enzyme (already corrected for back-exchange), corresponding to 41.9% and 33.0% of the total exchangeable amide hydrogens, respectively. Meanwhile, after 8 h incubation, the incorporation of 365 deuterons in the apoenzyme and 301 deuterons for the glyphosate-bound enzyme (already corrected for back-exchange) was detected, corresponding to 88.1% and 72.7% of the total amide hydrogens, respectively (see Figures S1−S3 in the Supporting Information).

The Localized H/D Exchange and Conformational Changes of MtEPSPS. The protein was completely mapped out by LC-ESI-MS and collision-induced dissociation (CID) of the proteolytic fragments. Peptic peptides were mass analyzed at various time points to probe the level of deuterium incorporated along the protein backbone in both the apoenzyme and the *Mt*EPSPS−glyphosate complex (see Figure S4 in the Supporting Information for an example of the LC-MS profile of peptic peptides and Figure S5 in the Supporting Information for examples of CID spectra of a peptic fragment from apo-*Mt*EPSPS in both the presence and absence of deuteration). These results were used to locate the differences in deuterium incorporation between the two protein forms. Digestion with pepsin produced 67 peptic peptides (Figure 4), which covered 98.5% of the protein sequence.

In order to show the localized deuterium incorporation after 1 min incubation at 25 °C, some individual peptic fragments representative of different regions of *Mt*EPSPS (fragments 83−94, 95−101, 122−127, 163−170, 341−349, and 382−389) were selected, and their time courses of deuteration are shown in Figure 5. The distribution of points in this figure shows increments in steps and apparently does not follow an exponential distribution; thus, the lines observed in this figure were manually traced point to point by using a flexible French curve ruler. In all the peptic fragments represented in Figure 5 the apoenzyme was more susceptible to deuteration than the glyphosate-bound enzyme. These results follow the same pattern observed for the global H/D exchange reported in Figure 3.

The H/D exchange rate constants were determined for a representative group of 23 peptic fragments, and the exchanging amide hydrogens were classified as fast, intermediate, and slow, as shown in Table 1 for the apoenzyme and in Table 2 for the glyphosate-bound enzyme. A general comparison of the two tables reveals that the values of the rate constants for the fast-exchanging hydrogens (K_{fast}) for the apo-*Mt*EPSPS are higher than the equivalent values

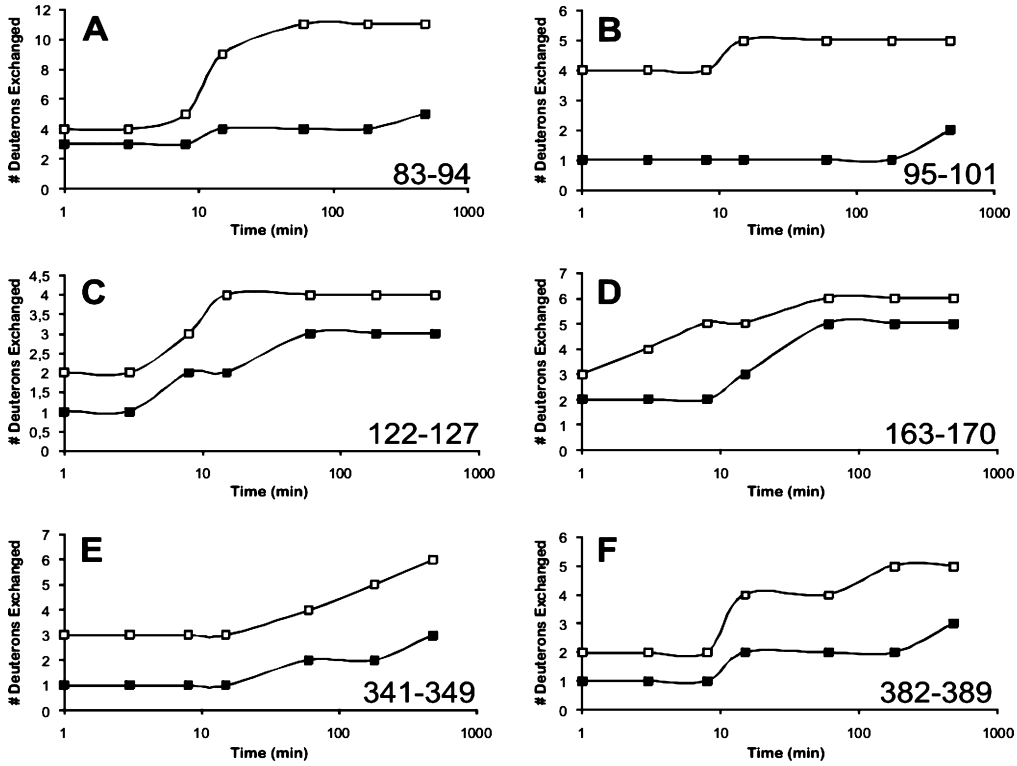

FIGURE 5: Normalized time course (at 25 °C and pH 6.9) for deuterium incorporation into six representative peptic fragments both for the apoenzyme (□) and for the glyphosate-bound enzyme (■).

Table 1: Constants of H/D Exchange Calculated According to Equation 2 and Number of Amide Hydrogens Exchanged in the Backbone of the Unliganded *Mt*EPSPS at Different Rates for Enzyme Incubated in the Presence of D_2O at 25 °C[a]

residues	N_{fast}	k_{fast} (min^{-1})	N_{int}	k_{int} (min^{-1})	N_{slow}	k_{slow} (min^{-1})
5−9	3.20 ± 0.55	2.00 ± 0.40	0.20 ± 0.04	0.10 ± 0.02	0.90 ± 0.02	0.002 ± 0.001
16−32	3.10 ± 0.60	1.87 ± 0.35	9.80 ± 1.75	0.65 ± 0.15	2.90 ± 0.05	0.006 ± 0.002
63−67	2.00 ± 0.45	1.25 ± 0.25	1.80 ± 0.35	0.12 ± 0.02	0.10 ± 0.02	0.001 ± 0.001
83−94	4.30 ± 0.80	2.70 ± 0.45	6.80 ± 1.25	0.45 ± 0.10		
95−101	3.90 ± 0.75	2.45 ± 0.50	2.10 ± 0.35	0.07 ± 0.01	0.20 ± 0.04	0.004 ± 0.001
122−127	3.30 ± 0.60	2.06 ± 0.40	1.90 ± 0.30	0.14 ± 0.02	0.20 ± 0.04	0.004 ± 0.001
146−155	5.10 ± 0.95	3.19 ± 0.65	2.70 ± 0.50	0.18 ± 0.03	1.20 ± 0.25	0.003 ± 0.001
163−170	3.70 ± 0.65	2.31 ± 0.45	3.10 ± 0.55	0.21 ± 0.04	0.40 ± 0.08	0.008 ± 0.002
171−176	2.40 ± 0.50	1.51 ± 0.30	2.80 ± 0.50	0.19 ± 0.03	0.10 ± 0.01	0.002 ± 0.001
208−214	4.30 ± 0.85	2.69 ± 0.55	1.90 ± 0.40	0.13 ± 0.02	0.20 ± 0.03	0.004 ± 0.001
269−279	5.10 ± 1.05	3.20 ± 0.60	3.80 ± 0.65	0.25 ± 0.04	1.20 ± 0.20	0.003 ± 0.001
281−287	4.70 ± 0.90	2.94 ± 0.55	1.10 ± 0.25	0.07 ± 0.01	0.10 ± 0.01	0.002 ± 0.001
300−308	5.10 ± 1.10	3.19 ± 0.60	2.20 ± 0.45	0.15 ± 0.03	1.00 ± 0.25	0.002 ± 0.001
309−317	4.90 ± 0.90	3.06 ± 0.55	2.30 ± 0.50	0.15 ± 0.03	1.10 ± 0.20	0.002 ± 0.001
313−319	2.00 ± 0.35	1.25 ± 0.25	2.80 ± 0.55	0.18 ± 0.35	1.30 ± 0.25	0.003 ± 0.001
322−331	5.20 ± 1.15	3.25 ± 0.60	1.40 ± 0.25	0.09 ± 0.20	2.30 ± 0.35	0.005 ± 0.002
341−349	2.80 ± 0.55	1.75 ± 0.35	5.30 ± 1.05	0.35 ± 0.07	0.20 ± 0.01	0.004 ± 0.001
367−373	2.20 ± 0.40	1.38 ± 0.25	3.30 ± 0.60	0.22 ± 0.04	0.70 ± 0.01	0.001 ± 0.001
382−389	4.10 ± 0.80	2.57 ± 0.50	1.80 ± 0.30	0.12 ± 0.02	1.10 ± 0.15	0.002 ± 0.001
393−398	1.90 ± 0.35	1.19 ± 0.25	0.90 ± 0.20	0.06 ± 0.01	2.10 ± 0.40	0.004 ± 0.001
406−412	3.20 ± 0.65	2.00 ± 0.40	2.30 ± 0.45	0.14 ± 0.02	0.80 ± 0.02	0.002 ± 0.001
420−429	3.70 ± 0.70	2.31 ± 0.40	3.10 ± 0.50	0.21 ± 0.04	1.90 ± 0.35	0.004 ± 0.001

[a] The constants were classified as "fast", "intermediate", and "slow" taking into account the experimental times determined to observe each group of H/D exchange, considering the following time windows: "fast" from 0 to 1.6 min, "intermediate" from 1.7 to 15 min, and "slow" for times longer than 15 min.

Table 2: Constants of H/D Exchange Calculated According to Equation 2 and Number of Amide Hydrogens Exchanged in the Backbone of the *Mt*EPSPS−Glyphosate Complex at Different Rates, Incubated in the Presence of D_2O at 25 °C[a]

residues	N_{fast}	k_{fast} (min^{-1})	N_{int}	k_{int} (min^{-1})	N_{slow}	k_{slow} (min^{-1})
5−9	1.80 ± 0.35	1.12 ± 0.34	0.70 ± 0.30	0.05 ± 0.10	1.90 ± 0.45	0.004 ± 0.001
16−32	2.10 ± 0.42	1.31 ± 0.41	4.80 ± 0.73	0.32 ± 0.20	8.80 ± 1.30	0.018 ± 0.003
63−67	2.20 ± 0.39	1.37 ± 0.42	1.00 ± 0.29	0.07 ± 0.02	0.90 ± 0.20	0.002 ± 0.001
83−94	4.20 ± 0.70	2.00 ± 0.50	2.90 ± 0.47	0.19 ± 0.40	4.10 ± 0.90	0.009 ± 0.002
95−101	1.70 ± 0.35	1.06 ± 0.29	0.30 ± 0.06	0.02 ± 0.01	3.80 ± 0.80	0.008 ± 0.002
122−127	1.60 ± 0.31	1.00 ± 0.22	1.10 ± 0.20	0.07 ± 0.01	2.20 ± 0.50	0.005 ± 0.001
146−155	3.20 ± 0.58	2.00 ± 0.38	1.30 ± 0.23	0.09 ± 0.02	4.80 ± 0.95	0.010 ± 0.003
163−170	2.10 ± 0.41	1.31 ± 0.36	2.00 ± 0.44	0.13 ± 0.26	3.30 ± 0.60	0.007 ± 0.002
171−176	2.10 ± 0.38	1.31 ± 0.34	1.20 ± 0.23	0.08 ± 0.03	1.90 ± 0.35	0.004 ± 0.001
208−214	2.10 ± 0.39	1.31 ± 0.35	1.80 ± 0. 35	0.12 ± 0.01	2.30 ± 0.40	0.005 ± 0.001
269−279	4.30 ± 0.75	2.69 ± 0.65	2.20 ± 0.45	0.15 ± 0.02	3.20 ± 0.60	0.007 ± 0.002
281−287	4.09 ± 0.67	2.56 ± 0.57	1.10 ± 0.30	0.07 ± 0.02	1.20 ± 0.30	0.003 ± 0.001
300−308	2.20 ± 0 42	1.37 ± 0.34	1.20 ± 0.34	0.08 ± 0.02	3.80 ± 0.70	0.008 ± 0.003
309−317	1.90 ± 0.37	1.19 ± 0.27	0.70 ± 0.21	0.05 ± 0.01	5.10 ± 1.05	0.010 ± 0.003
313−319	1.70 ± 0.34	1.06 ± 0.29	1.30 ± 0.39	0.09 ± 0.02	3.10 ± 0.55	0.006 ± 0.001
322−331	2.10 ± 0.42	1.31 ± 0.34	0.80 ± 0.02	0.05 ± 0,01	5.80 ± 1.10	0.012 ± 0.003
341−349	2.20 ± 0.39	1.37 ± 0.36	2.30 ± 0.43	0.15 ± 0.03	4.70 ± 0.90	0.010 ± 0.003
367−373	2.10 ± 0.38	1.31 ± 0.32	1.20 ± 0.26	0.08 ± 0.02	4.10 ± 0.85	0.009 ± 0.002
382−389	2.07 ± 0.39	1.25 ± 0.27	2.10 ± 0.45	0.14 ± 0.03	2.90 ± 0.50	0.006 ± 0.001
393−398	1.80 ± 0.35	1.12 ± 0.23	0.90 ± 0.03	0.06 ± 0.01	2.30 ± 0.45	0.005 ± 0.001
406−412	1.70 ± 0.34	1.06 ± 0.20	1.30 ± 0.25	0.09 ± 0.02	2.90 ± 0.60	0.006 ± 0.001
420−429	2.40 ± 0.43	1.50 ± 0.42	1.90 ± 0.37	0.13 ± 0.03	4.90 ± 0.65	0.010 ± 0.003

[a] The constants were classified as "fast", "intermediate", and "slow" taking into account the experimental times determined to observe each group of H/D exchange, considering the following time windows: "fast" from 0 up to 1.6 min, "intermediate" from 1.7 to 15 min, and "slow" for times longer than 15 min.

determined for the *Mt*EPSP−glyphosate complex; also, the number of slow-exchanging hydrogens (N_{slow}) for the apoenzyme is smaller than that determined for the glyphosate-bound enzyme, reflecting the effects of conformational changes induced by the inhibitor.

A comparison of the percentages of deuterium exchanges between the apoenzyme (Figure 6A) and glyphosate-bound enzyme (Figure 6B) as a function of time (1 min, 3 min, 8 min, 15 min, 1 h, 3 h, and 8 h) reveals that this value is clearly different for each enzyme form. The schedule represented in Figure 6 shows the primary sequence of *Mt*EPSPS, the secondary structures, and the color-coded representation of deuterium incorporation for both forms of *Mt*EPSPS at different incubation times. Initially, it should be emphasized that the comparison between the molecular models (Figures 1 and 6) for the open and closed enzyme conformations reveals that the secondary structures of both enzyme forms are slightly different from each other, indicating that *Mt*EPSPS undergoes some structural rearrangements after glyphosate binding. This also may be observed both for the apoenzyme (Figure 2A) and for the inhibitor-bound enzyme (Figure 2B) when the profiles of the folding units are split into the two domains. The apo-*Mt*EPSPS has two large domains, where domain 1 is comprised of units 1, 2, and 6 of $\beta\alpha\beta\alpha\beta\beta$-folds and domain 2 is comprised of three other $\beta\alpha\beta\alpha\beta\beta$-folding units, designated 3, 4, and 5 (Figure

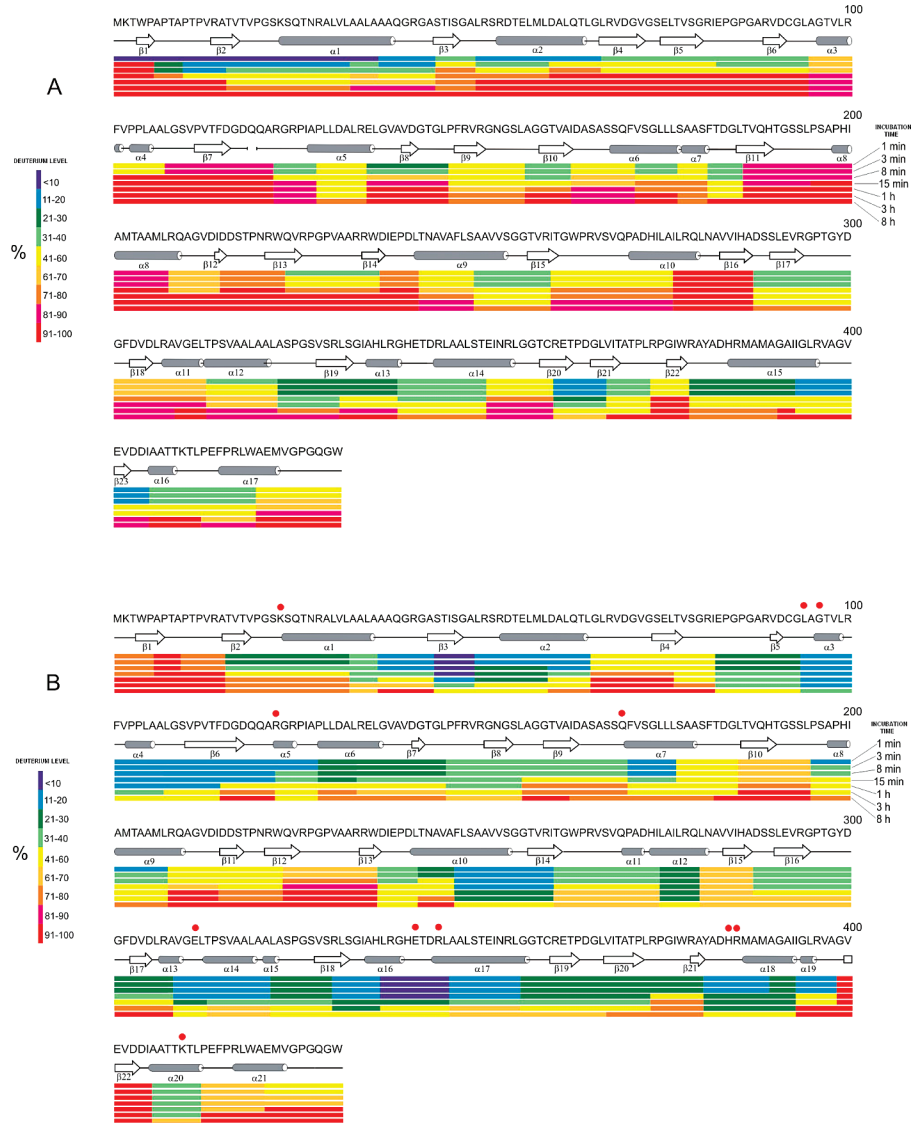

FIGURE 6: Schematic representation of the relative deuterium incorporation in each peptic fragment from different regions of *Mt*EPSPS both for the apoenzyme (A) and for the glyphosate-bound enzyme (B). The scheme shows the primary sequence of the enzyme, the secondary structure elements in each enzyme conformation, and a series of colored bars below the sequence to represent, in descending order, deuterium uptake at 1 min, 3 min, 8 min, 15 min, 1 h, 3 h, and 8 h. The dark blue color was used to represent the lowest level of deuterium incorporation, and a gradient of different colors shifting in direction to the red was used to represent the increasing deuterium incorporation, where red represents the highest level of deuterium incorporation. α-Helices are represented as cylinders, while β-strands are represented as arrows. The amino acid residues participating in the inhibitor binding site were assigned with red spots in the schematic (B).

2A). This pattern was slightly modified after the inhibitor binding to the enzyme; thus, units 1, 2, 3, and 5 maintained the $\beta\alpha\beta\alpha\beta\beta$-fold, while units 4 and 6 presented a $\beta\alpha\beta\alpha\beta\alpha$-fold (Figure 2B). It must be emphasized that the structural rearrangements exhibited by *Mt*EPSPS involved the splitting of some regions of loop/coil into α-helical elements, as reported for the region of Arg 122 to Arg 124 (which split into α5), the α-helices 6 and 7 (which merged and decreased the total extension, forming a single helix, α7), α-helix 10 (which split into helices 11 and 12), and β-strands 4, 6, and part of 5 (which split into coils/turns) (Figures 2 and 6).

In order to understand the localized conformational changes, the structure of *Mt*EPSPS was analyzed according to the folding organization of the enzyme in both forms, taking into account the elements of secondary structure of each folding unit, as represented in Figure 2. Thus, deuterium exchange was analyzed and expressed as a relative value for each region. The H/D exchanges undergone by both enzyme forms within the first minute of incubation at 25 °C are expressed in Figures 7 and 8 according to the different elements of secondary structure of each one of the folding units. Thus, Figure 7 shows the deuterium incorporation in the β-strands, which form the β-sheets of all 6-folding units, while Figure 8 shows the deuterium incorporation in all of the α-helical elements of the same 6-folding units.

In the search for possible correlations between the intensity of deuterium incorporation with changes in calculated structural parameters, the SASA values (for the total accessible area of all nitrogens from the backbones of each selected peptide) and the number of hydrogen bonds of the backbone nitrogens for some regions of the enzyme containing the amino acid residues of the glyphosate binding site were compared both in the unliganded *Mt*EPSPS and in the form complexed with the inhibitor. Thus, the regions covered by a group of six peptides, representative of a peptic digest of *Mt*EPSPS, were selected and analyzed for the structural

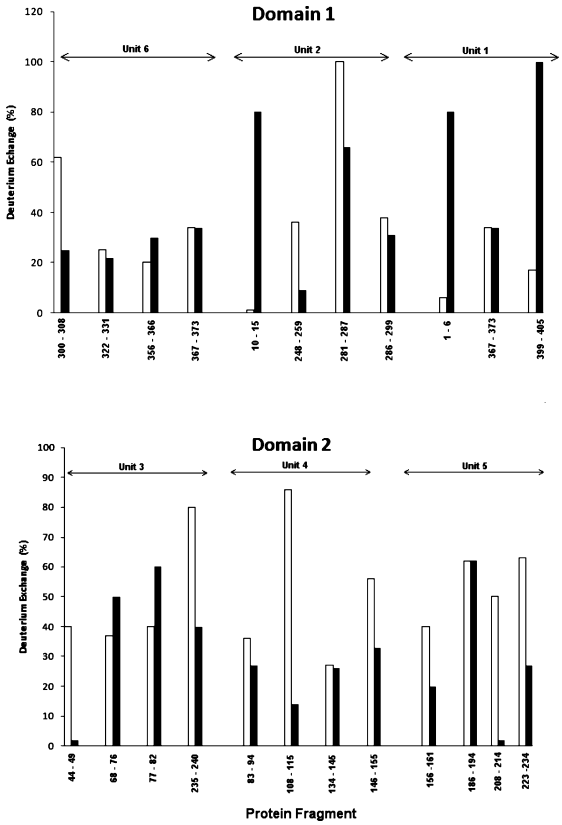

FIGURE 7: Deuterium incorporation in the β-strand elements of the secondary structure of *Mt*EPSPS, both for the apoenzyme (□) and for the glyphosate-bound enzyme (■) after 1 min incubation at 25 °C and pH 6.9. The β-strands were defined according to their location along the amino acid sequence and grouped according to their participation in the folding units from 1 to 6 and their position in domains 1 or 2.

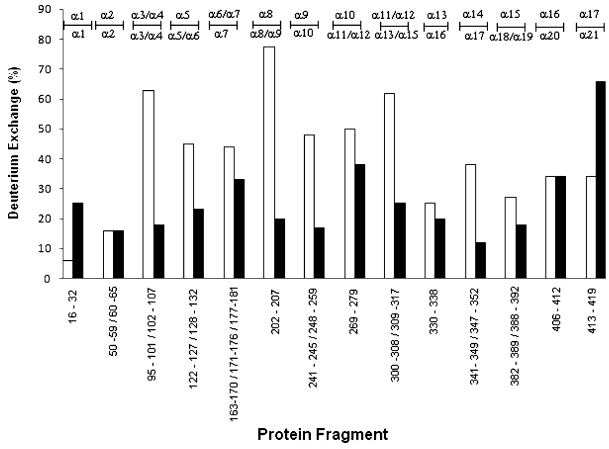

FIGURE 8: Deuterium incorporation in the α-helical elements of the secondary structure of *Mt*EPSPS, both for the apoenzyme (□) and for the glyphosate-bound enzyme (■) after 1 min incubation at 25 °C and pH 6.9. The α-helices were defined according to their location along the amino acid sequence from the N- to the C-terminal region. Above each group of bars, the position of the α-helix in the secondary structure is indicated: the upper indication corresponds to the position in the apoenzyme, while the lower indication corresponds to the position in the glyphosate-bound enzyme. To cover the complete extension of some α-helices, it was necessary to represent these structural elements with two or three continuous peptides, separated by slashes.

parameters mentioned above; the selected peptides represented the fragments 16−32 (α1), 116−121 (α5/α6), 122−127 (α7), 163−170 (α8), 195−200 (α15/α16), and 382−389 (α17). The results obtained are shown in Table 3. These results clearly show that within the first minute of incubation at 25 °C, the higher levels of deuterium incorporation in the apoenzyme are directly correlated to higher SASA values and inversely correlated with the number of calculated hydrogen bonds in these regions of the apoenzyme compared to the same positions in the inhibitor-bound form of the enzyme.

Studies of the conformational changes of the human retinoid-X receptor homodimer using the experimental approach used in the present study also reported that the decrease in deuterium incorporation in some regions of this protein may result from a reduction in the solvent-accessible area. The authors referred to the movements of the protein, i.e., the expansion (increasing the surface area accessible to the solvent) and/or the compaction (decreasing the surface area accessible to the solvent) of the secondary structure elements as "protein breathing", which sometimes may be related to changes of the percentage of each element of secondary structure, characteristic of each compact or expanded conformation (*25*).

Since *Mt*EPSPS undergoes extensive conformational changes due to inhibitor binding to the apoenzyme molecule, we decided to investigate the "protein breathing", i.e., the expansion and compaction, through measurements of the CD spectra of the open and closed forms of this enzyme. These results are represented in Figure 9. The CD technique was used to characterize the *Mt*EPSPS secondary structure content both in the absence and in the presence of the inhibitor. Figure 9 represents the *Mt*EPSPS CD spectra in both conditions, showing that they were slightly different from each other; however, α-helices seem to be the main secondary structure element in both forms. The secondary structure contents estimated by the CDNN deconvolution software (*36*) for the apoenzyme were 40% α-helices, 30% β-sheets, and 30% random coils, while the values for the glyphosate-bound enzyme were 57% α-helices, 23% β-sheets, and 20% random coils (error was less than 5%).

DISCUSSION

The Global H/D Exchange of MtEPSPS. The global mass changes in the apo-*Mt*EPSPS and in the *Mt*EPSPS−glyphosate complex following H/D exchange were determined by analyzing the intact protein by LC-ESI-MS; the masses of both enzyme forms increased with incubation time as shown in Figure 3. *Mt*EPSPS is comprised of 450 amino acid residues and considering the presence of 33 proline residues (which do not contribute amide hydrogens) and that side chain C- and N-terminal deuterons are removed by back-exchange with the quenching solution, the maximum number of exchangeable amide hydrogens in this protein is 415.

The results shown in Figure 3 clearly reveal the protective effect of the conformational changes induced by the complexation of glyphosate; after a 480 min incubation at 25 °C, 50 of the global amide hydrogens of the apoenzyme were protected from the solvent, while the access of the solvent to 114 amide hydrogens was prevented in the glyphosate-bound enzyme. Apparently, the complexation of the inhibitor by the enzyme prevented the solvation of a series of amino acid residues.

Table 3: Comparison of Experimental Deuterium Levels in Some Peptic Fragments from the Apoenzyme and Glyphosate-Bound Enzyme after 1 min at 25 °C and Changes in Some of the Structural Parameters

	deuterium level (no.)		SASA (Å)^2		no. of hydrogen bonds	
peptides	apoenzyme	glyphosate-bound enzyme	apoenzyme	glyphosate-bound enzyme	apoenzyme	glyphosate-bound enzyme
16−32 (α1)	3.1	2.1	18	12	13	14
116−121 (α5/α6)	4.2	0.9	41	25	1	4
122−127 (α7)	3.3	1.6	50	21	2	4
163−170 (α8)	3.7	2.1	90	24	3	5
195−200 (α15/α16)	4.1	2.2	89	4	1	3
382−389 (α17)	4.1	2.0	8	4	3	5

The general profile of the global deuterium incorporation in *Mt*EPSPS incubated at 25 °C (Figure 3) follows a biphasic kinetics, already observed for other enzymes (*46, 47*). However, neither the apoenzyme nor the complex enzyme−glyphosate seems to undergo thermal denaturation, but a local dynamic fluctuation within the protein, exposing the amide hydrogens to the classic mechanism of "slow exchanging". The curves shown in Figure 3 are approximately parallel to each other, indicating that both forms of the enzyme followed similar dynamic fluctuation processes, except that the rate of these processes seems to be faster in the apoenzyme. After 10 min at 25 °C, the deuterium incorporation became more pronounced in both forms of enzyme but was more pronounced in the apoenzyme.

The Localized H/D Exchange and Conformational Changes of MtEPSPS. Digestion with pepsin produced 67 peptides (Figure 4) covering 98.5% of the protein sequence. The analysis of deuterium incorporation in these peptic fragments follows the pattern already observed for the global H/D exchange shown in the Figure 3. The analysis of localized deuterium incorporation of some individual peptides from different regions of *Mt*EPSPS after 1 min incubation at 25 °C (Figure 5) revealed that the apoenzyme was more susceptible to deuteration than the glyphosate-bound enzyme.

At first, a comparison of the color-coded representations of deuterium incorporation for both enzyme forms reveals that the enzyme in the closed conformation (Figure 6B) contains many regions with lower deuterium incorporation than the enzyme in the open conformation (Figure 6A). Another aspect that stands out is the observation of conformational dynamics fluctuations in the unliganded form of *Mt*EPSPS, even under mild physicochemical conditions; i.e., some regions of apo-*Mt*EPSPS became more accessible to the solvent just by incubation at 25 °C in the absence of any ligand (Figure 6), without necessarily undergoing conformational changes. Thus, the N-terminal region of the apoenzyme, comprised of β-turn 1/loop/β-turn 2/loop/helix 1/loop/β-turn 3/loop/helix 2, and the C-terminal region, comprised of the helix 15/loop/β-turn 23/loop/helix 16/loop/helix 16, were relatively protected from access by the solvent within the first minute of incubation at 25 °C; however, these regions became flexible and highly accessible to the solvent after 15 min.

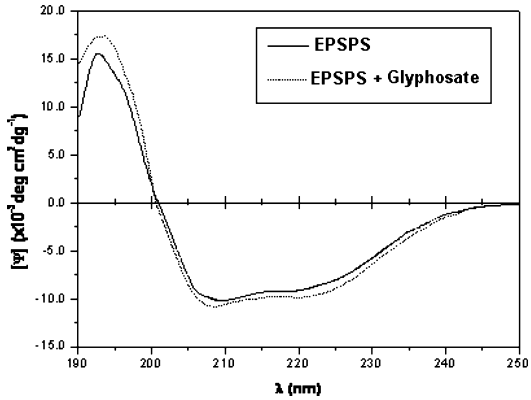

FIGURE 9: CD spectra obtained for *Mt*EPSPS in native conditions, both in the absence (—) and in the presence (•••) of glyphosate.

Several regions that were relatively accessible to the solvent (and/or not strongly stabilized by hydrogen bonding) in the apoenzyme became more protected from contact with the solvent (and/or more stable by the increasing in the number of amide hydrogens involved in hydrogen bonding) in the glyphosate-bound enzyme, such as fragments 16−32, 63−67, 83−94, 102−107, 108−115, 116−121, 122−127, 202−207, 223−234, 276−280, 281−287, 330−338, 335−345, and 374−378. The region constituted by fragments 10−15, 68−76, 77−82, and 399−405 became more accessible to the solvent in the ligand-bound form, when compared to the apoenzyme (Figure 6).

To interpret the results of Figure 7, it is important to emphasize that the β-sheets are shielding the two α-helices of each folding unit, causing a protective effect on the helices. The strands that form the β-sheet of each folding unit were individually represented in Figure 7. In domain 1, the binding of glyphosate to the apoenzyme caused an apparent decrease in solvent accessibility and, consequently, in the level of H/D exchange of the peptides represented by fragments 300−308 (unit 6) and 248−259, 281−287 (unit 2), while in domain 2, a similar effect was observed for the peptides represented by fragments 44−49 and 235−240 (unit 3), 83−94, 108−115, and 146−155 (unit 4) and 156−161, 208−214, and 223−234 (unit 5). Thus, a total of 13 β-strand elements became less exposed to the solvent after the binding of the inhibitor to the enzyme; it must be emphasized that 8 of these elements of secondary structure were localized in domain 2. In addition to this, other β-strand elements represented by fragments 356−366 (unit 6), 10−15 (unit 2), 1−6 and 399−405 (unit 1), and 68−76 and 77−82 (unit 3) underwent conformational changes that made them more exposed to the solvent.

These results permit us to conclude that, in domain 1 of *Mt*EPSPS, four β-strand elements became more exposed to the solvent, four other elements became less exposed, and the remaining elements did not undergo significant conformational changes due to glyphosate complexation by the enzyme (Figure 7). Meanwhile, in domain 2, eight β-strand elements became less exposed to the solvent due to inhibitor binding to the apoenzyme, two other structural elements became more accessible to the solvent, and the two remaining ones did not undergo significant conformational changes (Figure 7). As a general rule, it seems that inhibitor binding

to the enzyme causes a series of conformational changes at level of the β-strand elements, which probably makes the β-sheets from the folding units 3, 4, and 5 more compact in the glyphosate-liganded enzyme than in the apoenzyme, probably in order to protect the protein core, which was basically comprised of α-helices. The N- and C-terminal regions represented by fragments 1−6 and 399−405 (localized in unit 1 of domain 1) are among those regions of β-strand elements that became much more exposed to the solvent after the inhibitor binding to the enzyme.

Figure 8 shows the H/D exchange within the first minute of incubation at 25 °C for the 14 α-helical elements, positioned in the 6-folding units of the enzyme, both in the presence and in the absence of glyphosate. A detailed analysis of these results reveals that there is a pattern of conformational changes in which the two α-helical elements represented by fragments 16−32 (α1 in the apoenzyme) and 413−419 (α17 in the apoenzyme) constitute external flexible flanks proximal to the N- and C-terminal regions, respectively, which are more exposed to solvent in the presence of glyphosate. In addition to this, two other α-helical elements from the same regions, represented by fragments 50−59/60−65 (α2 in the apoenzyme) and 406−412 (α16 in the apoenzyme), apparently did not change their profile of H/D exchange; these structural elements seem to constitute two rigid flanks. However, 10 out of the 14 α-helical elements that exist in the apoenzyme became less exposed to the solvent after the binding of glyphosate, resulting in their apparent compaction with a consequent decrease in the level of H/D exchange: 95−101/102−107 (α3/α4 in the apoenzyme), 122−127/128−132 (α5 in the apoenzyme), 163−170/171−176/177−181 (α6/α7 in the apoenzyme), 202−207 (α8 in the apoenzyme), 241−245/248−259 (α9 in the apoenzyme), 269−279 (α10 in the apoenzyme), 300−308/309−317 (α11/α12 in the apoenzyme), 330−3339 (α13 in the apoenzyme), 341−349/347−352 (α14 in the apoenzyme), and 382−389/388−392 (α15 in the apoenzyme) (Figure 8).

The amino acid residues participating in the glyphosate binding site are Lys^{23}, Leu^{94}, Gly^{96}, Arg^{124}, Gln^{169}, Glu^{311}, Glu^{341}, Arg^{344}, His^{384}, Arg^{385} and Lys^{410} (*2*); their positions are indicated with red spots in Figure 6B. A careful comparative analysis of Figure 6A,B reveals that the most of peptic fragments containing these amino acid residues exhibited reduced deuterium incorporation in their amide hydrogens after glyphosate complexation to the apoenzyme, probably in order to permit the enzyme to accommodate the inhibitor in the correct orientation (in its extended conformation (*29*)) within the binding site. These regions are represented by peptic fragments 83−94 (loop/β-strand 3 in the apoenzyme), 95−101 (α3/α4 in the apoenzyme), 122−127 (α5 in the apoenzyme), 163−170 (α6/α7 in the apoenzyme), 309−317 (α11/α12 in the apoenzyme), 341−349 (α14 in the apoenzyme), and 382−389 (α15 in the apoenzyme).

Panels A and B of Figure 10 are representations of the 3-D structures of apo-*Mt*EPSPS after 1 min (A) and after 1 h (B) incubation at 25 °C. It is possible to observe that domain 1 (the left one) contains a reduced number of elements of secondary structure presenting fast-exchanging amide hydrogens, while domain 2 (the right one) contains a larger number of structural elements that have fast-exchanging amide hydrogens, mainly after 1 h incubation. Panels C and D of Figure 10 show the 3-D structures of the glyphosate-bound enzyme after 1 min (C) and after 1 h (D) incubation at 25 °C. Comparison between the structures of apo-*Mt*EPSPS (Figure 10A) and the glyphosate-bound EPSPS (Figure 10C) after 1 min incubation and between the structures of apo-*Mt*EPSPS (Figure 10B) and the glyphosate-bound *Mt*EPSPS (Figure 10D) after 1 h incubation clearly reveals the effects of the conformational changes induced by inhibitor binding to the enzyme, which decreases the relative rates of H/D exchange.

An important aspect which must be emphasized is that the results described and discussed above about the conformational dynamics of *Mt*EPSPS fit very well to the molecular models proposed for both the open and closed conformations of enzyme and may be used to validate them.

A detailed analysis of Tables 1 and 2 reveals that the rate constants of H/D exchange for the fast-exchanging hydrogens present the same order of magnitude generally observed for peptides fully exposed to the solvent in previous publications [49, 50]. The half-lives for the slow-exchanging peptides reported in both tables ranged from 15.1 to 480 min, indicating that these hydrogens originated from regions that are structurally stable. A direct comparison of the numbers of slow exchanging hydrogens (N_{slow}) experimentally observed for the same peptides from the apo-*Mt*EPSPS and the complex *Mt*EPSPS−glyphosate reveals that these numbers increased after inhibitor binding to the enzyme, indicating that the secondary structure of the enzyme became more stable due to inhibitor complexation.

The relationship between deuterium incorporation, solvent accessibility to the backbone nitrogens, and the number of amide hydrogen involved in the formation of hydrogen bonds to stabilize the secondary structure is presented in Table 3. These results clearly show that within the first minute of incubation at 25 °C, the levels of deuterium incorporation are correlated with higher SASA values for the nitrogens from the backbone and inversely correlated with the number of hydrogen bonds in these regions. Thus, it seems that, as a general rule, *Mt*EPSPS in the absence of glyphosate (or its substrates) adopts an open conformation, in which the regions containing the binding site residues contain large areas of solvent accessibility that are stably maintained by a reduced number of hydrogen bonds. However, as the enzyme binds to its inhibitor, the enzyme changes its conformation to a closed form, in which the regions containing the amino acid residues of the binding site become more compact, decreasing the SASA values. Apparently, the inhibitor-induced enzyme compaction requires a higher number of hydrogen bonds to keep the structure stable than is required in the apoenzyme. The slow exchanging hydrogens (as those identified in Tables 1 and 2) may be involved with the formation of hydrogen bonds, which stabilize the secondary structure of the protein (*35*); thus, the higher values of N_{slow} for the inhibitor-bound enzyme (Table 2) compared to the apoenzyme (Table 1) corroborate the hypothesis that the closed and compact conformation of the liganded enzyme is more stable than the open conformation of the apoenzyme.

Considering that *Mt*EPSPS changes from an open to a closed conformation due to inhibitor complexation, which requires the compaction of most of the α-helices and some β-strands present in the 6-folding units and the occurrence of some structural rearrangements at level of the secondary

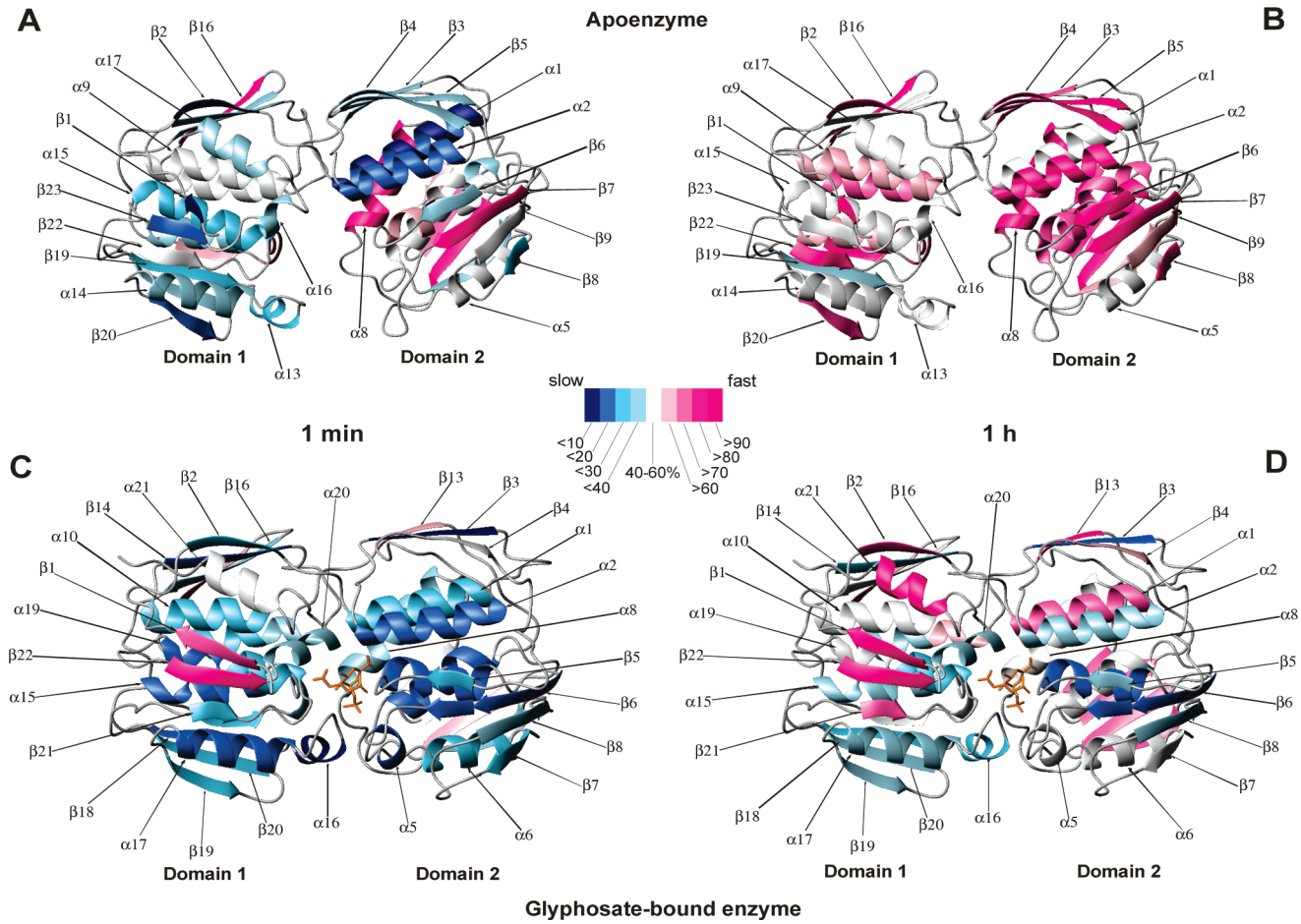

FIGURE 10: Relative H/D exchange behavior mapped onto the three-dimensional structures of the apo-*Mt*EPSPS after 1 min (A) and 1 h (B) incubation at 25 °C and pH 6.9 and for the glyphosate-bound *Mt*EPSPS after 1 min (C) and 1 h (D) incubation at 25 °C and pH 6.9. The dark blue color was used to represent the lowest level of deuterium incorporation, and a gradient of different colors shifting in direction to the red was used to represent the increasing deuterium incorporation, where red represents the highest level of deuterium incorporation.

structure, it was necessary to analyze the content of α-helices and *β*-sheets of the enzyme, in both the open and closed conformations, through CD analysis. The deconvolution of the spectra of Figure 9 revealed that the complexation of the ligand by the apoenzyme led to an increase in the content of α-helices, with a consequent decrease in the content of *β*-sheets and random coils. The contents of α-helices and *β*-sheets obtained for *Mt*EPSPS (both in open and closed conformations) are higher than those values previously reported for the same enzyme from other species in the crystal form; thus, *Ec*EPSPS and *Sp*EPSPS crystallographic structures with different ligands deposited in the Protein Data Bank contained 30% α-helices and 23% *β*-sheets (PDB access codes 1RF4, 1RF5, and 1RF6 (*4*) and 1G6S and 1G6T (*15*)). A possible explanation for the different amounts of helices and sheets described above may be due to the fact that the secondary structure of *Mt*EPSP was investigated into aqueous solution, where the proteins structures have a high degree of freedom to assume different conformations, with higher contents of helices and sheets. Meanwhile, the secondary structure of *Ec*EPSP and *Sp*EPSPS were determined from crystal structures, where there are some spacial restrictions to fit the protein molecules to an specific crystal packing, limiting the contents of helices and sheets to values more reduced than those observed in solution.

CONCLUSIONS

The results above are consistent with the hypothesis that *Mt*EPSPS undergoes extensive conformational changes when the apoenzyme complexes glyphosate in the inhibitor binding site, changing from the open to the closed conformation, which seems to be characterized by an increase in the percentage of α-helices and a decrease in the percentage of *β*-sheets. If these observations are correlated with the reduced level of H/D exchange presented by the liganded enzyme compared to its apo form, it is possible to speculate that enzyme compaction may be strongly associated with the rearrangements of the secondary structure after glyphosate binding.

The fact that in *Mt*EPSPS there is almost 50% deuteration of many α-helices after only 1 min implies that the whole protein structure is very flexible. Generally, the helices are the most stable elements of secondary structure of proteins. The great flexibility of the *Mt*EPSPS molecule may be part the mechanism for the rapid interconversion between different conformations of this protein, through the rearrangement of its secondary structure. If it were too stable, it could not make this transition as easily.

In addition to this, in *Mt*EPSPS the *β*-sheets are externally positioned in the enzyme molecule, protecting the helices in the core of the molecule from solvent access. Considering

that 10 out of the 14 α-helices and 13 out of the 23 β-sheets of *Mt*EPSPS became less accessible to the solvent after the inhibitor binding, one may conclude that there was the compaction of 71% of the α-helices and 57% of the β-sheets as a consequence of glyphosate binding to the enzyme, increasing the shielding effect against solvent access to the core of enzyme.

Apparently, *Mt*EPSPS undergoes a series of inhibitor-induced conformational changes, which result in synergistic effects that prevent solvent access to the core of molecule, especially in the cleft region. The binding of S3P by the enzyme requires the complexation of three molecules of water to stabilize the substrate in its binding site (*13*); thus, the glyphosate-induced compaction of specific elements of secondary structure in the *Mt*EPSPS molecule may be both part of the mechanism of inhibition required to prevent the hydration of the substrate binding site and also required to induce the cleft closure to avoid the substrate entrance.

The monitoring of amide H/D exchange with ESI-mass spectrometry applied to full-length *Mt*EPSPS in the apo- and inhibitor-bound states has provided a perspective on the solution dynamics of the enzyme and the conformational changes induced by inhibitor binding. The technique, which employed differences in peptide mass with differential exposures to D_2O, permitted us to analyze the native enzyme under two different conformations. Studies in solution may circumvent some limitations that constrain the enzyme molecules in solid states including stereo effects that may be induced by crystal packing or even artifacts from the position of symmetry-related molecules in crystal structures. By mapping the structural information gained from the H/D exchange monitored by ESI mass spectrometry experiments onto the 3-D structure of *Mt*EPSPS, it was possible to define some structural elements of the enzyme molecule that are important for understanding glyphosate docking onto the enzyme and also the prevention of the substrate binding by glyphosate.

The results also permitted a dynamic structural view of the glyphosate-induced fit in *Mt*EPSPS, revealing dynamic states and fluctuating movements in the vicinity of the binding sites for unliganded enzyme.

SUPPORTING INFORMATION AVAILABLE

Five figures as described in the text. This material is available free of charge via the Internet at http://pubs.acs.org.

REFERENCES

1. World Health Organization, Global Tuberculosis Control, WHO Report 2001, Geneva, Switzerland, WHO/CDS/TB/2001.287.
2. Pereira, J. H., Canduri, F., Oliveira, J. S., Silveira, N. J. F., Basso, L. A., Palma, M. S., Jr., and Santos, D. S. (2003) Structural bioinformatics study of EPSP synthase from *Mycobacterium tuberculosis*. *Biochem. Biophys. Res. Commun. 312*, 608–614.
3. Du, W., Wallis, N. G., Mazzulla, M. J., Chalker, A. F., Zhang, L., Liu, W. S., Kallender, H., and Payne, D. J. (2000) Characterization of *Streptococcus pneumoniae* 5-enolpyruvylshikimate 3-phosphate synthase and its activation by univalent cations. *Eur. J. Biochem. 267*, 222–227.
4. Park, H., Hilsenbeck, J. L., Kim, H. J., Shuttleworth, W. A., Park, Y. H., Evans, J. N., and Kang, C. (2004) Structural studies of *Streptococcus pneumoniae* EPSP synthase in unliganded state, tetrahedral intermediate-bound state and S3P-GLP-bound state. *Mol. Microbiol. 51*, 963–971.
5. Roberts, F., Roberts, C. W., Johnson, J. J., Kyle, D. E., Krell, T., Coggins, J. R., Coombs, G. H., Milhous, W. K., Tzipori, S., Ferguson, D. J. P., Chakrabarti, D., and McLeod, R. (1998) Evidence for the shikimate pathway in apicomplexan parasites. *Nature 393*, 801–805.
6. Herrmann, K. M., and Weaver, L. M. (1999) The shikimate pathway. *Annu. Rev. Plant Physiol. Plant Mol. Biol. 50*, 473–503.
7. Stallings, W. C., Abdel-Meguid, S. S., Lim, L. W., Shieh, H., Dayringer, H. E., Leimgruber, N. K., Stegeman, R. A., Anderson, K. S., Sirorski, J. A., Padgette, S. R., and Kishore, G. M. (1991) Structure and Topological Symmetry of the Glyphosate Target 5-Enolpyruvylshikimate-3-Phosphate Synthase: A Distinctive Protein Folding. *Proc. Natl. Acad. Sci. U.S.A. 88*, 5046–5050.
8. Bourenkov, G. P., Kachalova, G. S., Strizhov, N., Bruning, M., Vagin, A., and Bartunik, H. D. (2006)*Mycobacterium tuberculosis* Epsp Synthase in Unliganded State, Protein Data Bank code 2bjb (http://www.rcsb.org/pdb/explore/explore.do?structureId=2BJB).
9. Marques, M. R., Pereira, J. H., Oliveira, J. S., Canduri, F., Basso, L. A., Santos, D. S., Azevedo Junior, W. F., and Palma, M. S. (2007) The inhibition of 5-enolpyruvylshikimate-3-phosphate synthase. *Curr. Drug Targets 8*, 445–457.
10. Stauffer, M. E., Young, J. K., and Evans, J. N. S. (2001) Shikimate-3-phosphate Binds to the Isolated N-Terminal Domain of 5-Enolpyruvylshikimate-3-phosphate synthase. *Biochemistry 40*, 3951–3957.
11. Studelska, D. R., Klug, C. A., Beusen, D. D., McDowell, L. M., and Schaefer, J. (1996) Long-Range Distance Measurements of Protein Binding Sites by Rotational-Echo Double-Resonance NMR. *J. Am. Chem. Soc. 118*, 5476–5477.
12. Coggins, J. R., Abell, C., Evans, L. B., Frederickson, M., Robinson, D. A., Roszak, A. W., and Laptorn, A. P. (2003) Experiences with the shikimate-pathway enzymes as targets for rational drug design. *Biochem. Soc. Trans. 31*, 548–552.
13. McDowell, L. M., Studelska, D. R., Poliks, B., O'Connor, R. D., and Schaefer, J. (2004) Characterization of the complex of a trifluoromethyl-substituted shikimate-based bisubstrate inhibitor and 5-enolpyruvylshikimate-3-phosphate synthase by REDOR NMR. *Biochemistry 43*, 6606–6611.
14. Priestman, M. A., Healy, M. L., Becker, A., Alberg, D. G., Barlett, P. A., Lushington, G. H., and Schonbrunn, E. (2005) Interaction of phosphonate analogues of the tetrahedral reaction intermediate with 5-enolpyruvylshikimate-3-phosphate synthase in atomic detail. *Biochemistry 44*, 3241–3248.
15. Schönbrunn, E., Eschenburg, S., Shutterworth, W. A., Schloss, J. V., Amrhein, N., Evans, J. N. S., and Kabsch, W. (2001) Interaction of the herbicide glyphosate with its target enzyme 5-enolpyruvylshikimate 3-phosphate synthase in atomic detail. *Proc. Natl. Acad. Sci. U.S.A. 98*, 1376–1380.
16. Eschenburg, S., Kabsch, W., Healy, M. L., and Schönbrunn, E. (2003) A new view of the mechanisms of UDP-N-acetylglucosamine enolpyruvyl transferase (MurA) and 5-enolpyruvylshikimate-3-phosphate synthase (AroA) derived from X-ray structures of their tetrahedral reaction intermediate states. *J. Biol. Chem. 278*, 49215–49222.
17. Stauffer, M. E., Young, J. K., Helms, G. L., and Evans, J. N. S. (2001) Chemical shift mapping of shikimate-3-phosphate binding to the isolated N-terminal domain of 5-enolpyruvylshikimate-3-phosphate synthase. *FEBS Lett. 499*, 182–186.
18. Rogers, S. G., Brand, L. A., Holder, S. B., Sharps, E. S., and Brackin, M. J. (1983) Experiences with the shikimate-pathway enzymes as targets for rational drug design. *Appl. Environ. Microbiol. 46*, 37–43.
19. Brown, K. A., Carpenter, E. P., Watson, K. A., Coggins, J. R., Hawkins, A. R., Koch, M. H. J., and Svergun, D. I. (2003) Twists and turns: A tale of two shikimate-pathway enzymes. *Biochem. Soc. Trans. 31*, 543–547.
20. Franz, J. E., Mao, M. K., and Sikorski, J. A. (1997) *Glyphosate: A Unique Global Herbicide*, American Chemical Society, Washington, DC.
21. Priestman, M. A., Funke, T., Singh, I. M., Crupper, S. S., and Schönbrunn, E. (2005) 5-Enolpyruvylshikimate-3-phosphate synthase from *Staphylococcus aureus* is insensitive to glyphosate. *FEBS Lett. 579*, 728–732.
22. McConkey, G. A., Rogers, M. J., and McCutchan, T. F. (1997) Inhibition of *Plasmodium falciparum* Protein Synthesis. *J. Biol. Chem. 272*, 2046–2049.
23. Kohler, S., Delwiche, C. F., Denny, P. W., Tilney, L. G., Webster, P., Wilson, R. J., Palmer, J. D., and Roos, D. S. (1997) A plastid of probable green algal origin in apicomplexan parasites. *Science 275*, 1485–1489.

24. Shi, J. S., Koeppe, J. R., Komives, E. A., and Paylor, P. (2006) Ligand-induced conformational changes in the Acetylcholine-binding Protein Analyzed by Hydrogen-deuterium Exchange Mass Spectrometry. *J. Biol. Chem. 281*, 12170–12177.
25. Yan, X., Broderick, D., Leid, M. E., Schmerlik, M. I., and Deizer, M. L. (2004) Dynamics and Ligand-Induced Solvent Accessibility Changes in Human Retinoid X Receptor Homodimer determined by Hydrogen Deuterium Exchange and Mass Spectrometry. *Biochemistry 43*, 909–917.
26. Englander, J. J., Rogero, J. R., and Englander, S. W. (1985) Protein hydrogen exchange studied by the fragment separation method. *Anal. Biochem. 147*, 234–244.
27. Hochrein, J. M., Wales, T. E., Lerner, E. C., Schiavone, A. P., Smithgall, T. E., and Engen, J. R. (2006) Conformational features of the full length HIV and SIV Nef proteins by mass spectrometry. *Biochemistry 45*, 7733–7739.
28. Wales, T. E., and Engen, J. R. (2006) Hydrogen exchange mass spectrometry for the analysis of protein dynamics. *Mass Spectrom. Rev. 25*, 158–170.
29. Funke, T., Han, H., Healy-Friend, M. L., Fischer, M., and Schöbrun, E. (2006) Molecular basis for the herbicide resistance of Roundup Ready crops. *Proc. Natl. Acad. Sci. U.S.A. 103*, 13010–13015.
30. Oliveira, J. S., Pinto, C. A., Basso, L. A., and Santos, D. S. (2001) Cloning and Overexpression in Soluble Form of Functional Shikimate Kinase and 5-Enolpyruvylshikimate-3-Phosphate Synthase Enzymes from *Mycobacterium tuberculosis*. *Protein Expression Purif. 22*, 430–435.
31. Oliveira, J. S., Mendes, M. A., Palma, M. S., Basso, L. A., and Santos, D. S. (2003) One-step purification of 5-enolpyruvylshikimate-3-phosphate synthase enzyme from *Mycobacterium tuberculosis*. *Protein Expression Purif. 28*, 287–292.
32. Pace, C. N., Vajdos, F. L., Grimsley Fee, G., and Gray, T. (1995) How to measure and predict the molar absorption coefficient of a protein. *Protein Sci. 4*, 2411–2423.
33. Zhang, Z., and Smith, D. L. (1993) Determination of amide hydrogen exchange by mass spectrometry: A new tool for protein structure elucidation. *Protein Sci. 2*, 522–531.
34. Wintrode, P. L., Keneth, F. L., Vierling, E., Smith, J. B., and Smith, D. L. (2003) Solution structure and dynamics of a heat shock protein assembly probed by hydrogen exchange and mass spectrometry. *Biochemistry 42*, 10667–10673.
35. Tsuitsui, Y., Gersheson, A., and Wintrode, P. (2006) The conformational dynamics of a metastable Serpin studied by hydrogen exchange and mass spectrometry. *Biochemistry 45*, 6561–6569.
36. Böhm, G., Muhr, R., and Jaenicke, R. (1992) Quantitative analysis of protein far UV circular dichroism spectra by neural networks. *Protein Eng. 5*, 191–195.
37. Sali, A., and Blundell, T. T. (1993) Comparative protein modelling by satisfaction of spatial restraints. *J. Mol. Biol. 234*, 779–815.
38. Uchoa, H. B., Jorge, G. E., da Silveira, N. J., Camera, J. C., Canduri, F., and de Azevedo, W. F. (2004) Parmodel: a web server for automated comparative modeling of proteins. *Biochem. Biophys. Res. Commun. 325*, 1481–1486.
39. Schönbrunn, E., Eschenburg, S., Shuttleworth, W. A., Schloss, J. V. N., Amrhein, N., Evans, J. N. S., and Kabsch, W. (2001) Interaction of the herbicide glyphosate with its target enzyme 5-enolpyruvylshikimate 3-phosphate synthase in atomic detail. *Proc. Natl. Acad. Sci. U.S.A. 98*, 1376–1380.
40. Braun, W., and Go, N. (1985) Calculation of protein conformations by proton−proton distance constraints. A new efficient algorithm. *J. Mol. Biol. 186*, 611–626.
41. Lee, B., and Richards, F. M. (1971) The interpretation of protein structures: estimation of static accessibility. *J. Mol. Biol. 55*, 379–400.
42. Richards, F. M. (1977) Areas, volumes, packing and protein structure. *Annu. Rev. Biophys. Bioeng. 6*, 151–176.
43. Connolly, M. L. (1983) Analytical molecular surface calculation. *J. Appl. Crystallogr. 16*, 548–558.
44. Fraczkiewicz, R., and Braun, W. (1998) Exact and efficient analytical calculation of the accessible surface areas and their gradients for macromolecules. *J. Comput. Chem. 19*, 319–333.
45. Hooft, R. W. W., Sander, C., and Vriend, G. (1996) Positioning hydrogen atoms by optimizing hydrogen-bond networks in protein structures. *Proteins 26*, 363–376.
46. Deng, Y., and Smith, D. L. (1998) Identification of unfolding domains in large proteins by their unfolding rates. *Biochemistry 37*, 6256–6262.
47. Kim, M. Y., Maier, C. S., Reed, D. J., and Deinzer, M. L. (2002) Conformational changes in chemically modified *Escherichia coli* thioredoxin monitored by H/D exchange and electrospray ionization mass spectrometry. *Protein Sci. 11*, 1320–1329.

BI800134Y